Proceedings of the ASME 2018 Internal Combustion Fall Technical Conference
ICEF2018
November 4-7, 2018, San Diego, CA, USA

ICEF2018-9605

PREDICTION OF CYCLIC VARIABILITY AND KNOCK-LIMITED SPARK ADVANCE (KLSA) IN SPARK-IGNITION (SI) ENGINE

Zongyu Yue
Argonne National Laboratory
Lemont, IL, USA

K. Dean Edwards
Oak Ridge National Laboratory
Oak Ridge, TN, USA

C. Scott Sluder
Oak Ridge National Laboratory
Oak Ridge, TN, USA

Sibendu Som
Argonne National Laboratory
Lemont, IL, USA

ABSTRACT

Engine knock remains one of the major barriers to further improve thermal efficiency of Spark Ignition (SI) engines. Knock can be suppressed by lowering the compression ratio, or retarding the spark ignition timing, however, at an expense of efficiency penalty. SI engine is usually operated at knock-limited spark advance (KLSA) to achieve possibly maximum efficiency with given engine hardware and fuel properties, such as Research Octane Number (RON), Motor Octane Number (MON), and heat of vaporization, etc. Co-optimization of engine design and fuel properties is promising to improve the engine efficiency and predictive CFD models can be used to facilitate this optimization process. However, difficulties exist in predicting KLSA in CFD simulations. First, cyclic variability of SI engine demands that multi-cycle results are required to capture the extreme conditions. Secondly, Mach Courant-Friedrichs-Lewy (CFL) number of 1 is desired to accurately predict the knock intensity (KI), resulting in unaffordable computational cost, especially for multi-cycle simulations. In this study, a new approach to numerically predict KLSA using large Mach CFL number of 50 is proposed. This approach is validated against experimental data for a boosted Direct Injection Spark Ignition (DISI) engine at multiple loads and spark timings. G-equation combustion model coupled with well-mixed chemical kinetic model are used to predict the turbulent flame propagation and end-gas auto-ignition, respectively. Simulations run for 10 consecutive engine cycles at each condition. The results show good agreement between model predictions and experiments in terms of cylinder pressure, combustion phasing and cyclic variation. Engine knock is predicted with early spark ignition timing, indicated by significant pressure wave oscillation and end-gas heat release. Maximum Amplitude of Pressure Oscillation (MAPO) analysis is performed to quantify the KI, and the slope change point in KI extrema is used to indicate the KLSA accurately. Using a smaller Mach CFL number of 5 also results in the same conclusions thus demonstrating that this approach is insensitive to the Mach CFL number. The use of large Mach CFL number allows us to achieve fast turn-around time for multi-cycle engine CFD simulations.

INTRODUCTION

Motor gasoline fuel accounted for about 58.8% of total U. S. transportation energy use in 2017 [1] and is expected to continuously dominate the transportation market in the near future. Improvement in the thermal efficiency of gasoline spark-ignition (SI) engine is therefore critical to the reduction of total energy consumption and CO_2 emission. Engine knock has long been an issue for SI engines and one of the major barriers to achieving higher thermal efficiency. It is generally understood that knock is an abnormal combustion phenomenon that is caused by auto-ignition of fuel/air mixture in the end-gas prior the arrival of the spark-ignited propagating flame. The auto-ignition in the end-gas causes rapid heat release and sets off pressure waves fluctuating inside the cylinder, which produces noise and could lead to severe damage of the engine components. The recent trend of downsizing and turbocharging engines in the automotive industry offers the benefit of improved fuel economy and increased power density. However, it also increases the knock propensity by running engine at in-cylinder conditions that favors end-gas auto-ignition.

Retarding spark timing is an effective method of knock suppression. However, late spark timing usually leads to degraded engine performance and thermal efficiency due to non-ideal combustion phasing. Use of high knock-resistant fuel can extend the range of knock-free stable conditions and allow the knock-limited spark advance (KLSA) to be as close to its optimum point as possible under knock-limited conditions. Research Octane Number (RON) [2] and Motor Octane Number (MON) [3] are the most used rating methods for knock resistance of fuels in SI engines. A fuel is rated by comparing its knocking behavior against primary reference fuels (PRF) in the RON and MON tests, respectively. A practical fuel generally has different values for its RON and MON, and the difference is defined as octane sensitivity, S = RON - MON, while PRF has an octane sensitivity of 0 by definition. It is well known that neither RON nor MON can truly reflect the anti-knock quality of fuels used in modern engines [4][5], and much effort have been focused on refining methods for anti-knock rating and its sensitivity on engine operating conditions[4][6][7][8][9].

Computational Fluid Dynamics (CFD) has proved to be an effective tool for engine combustion research, and has also been applied to understanding the knock phenomenon. Eckert et al. [10] implemented several sub-models into the KIVA-3V code to predict the occurrence of knock in SI engines. A Lagrangian particle ignition model was used to capture the spark ignition and initial flame development. The propagation of regular flame was modeled using the characteristic-time combustion (CTC) model, and the end-gas auto-ignition was modeled using Shell ignition model with reduced chemical mechanism. This approach was tested for three different engines at non-knocking and knocking conditions, and was shown to be able to predict knock occurrence reasonably well. Liang et al. [11] used the G-equation combustion model coupled with detailed chemical kinetics to simulate a boosted Direct Injection Spark Ignition (DISI) engine, and studied knock mitigation strategies via cooled exhaust gas recirculation (EGR) and split fuel injection. This hybrid approach has been widely adopted for simulation of engine knock since then [12][13][15]. Shao et al. [12][13] used consumption of intermediate species HO_2 as an indicator of knock occurrence and invested the effect of gas addition on knock suppression. Pan et al. [14] performed Large Eddy Simulation (LES) engine simulation, and successfully captured normal knock by advancing spark timing, as well as super knock by reducing fuel octane number. Recently, a virtual Cooperative Fuel Research (CFR) engine CFD model was developed by Pal et al. [15] using a commercial software, Converge [16] to predict knocking combustion. Mach Courant-Friedrichs-Lewy (CFL) number of 1 was used to improve the accuracy in pressure wave prediction. Maximum amplitude of pressure oscillation (MAPO) analysis of the in-cylinder local pressure was performed and a criterion of 0.5 bar in knock intensity (KI) was adopted to capture the critical compression ratio of knock onset.

Although the studies reviewed above show promising results on qualitative and quantitative knock prediction, they did not account for cycle-to-cycle variation (CCV), which is another intrinsic feature of SI combustion. The cause of CCV is a combination of factors such as variations in in-cylinder flow, mixture inhomogeneity, turbulence intensity and spark discharge characteristics [17], which can also effect the knock propensity. CCV has drawn increasing interest among the CFD modeling community due to its importance in understanding SI combustion, as well as the continuous advancement in computational capabilities. It is generally accepted that LES methodology is the proper method to study CCV due to its transient and stochastic nature [18][19][20][21][22]. However, several studies observed CCV in multi-cycle Reynolds-Averaged Navier-Stokes (RANS) simulation, which is attributed to the use of fine mesh resolution and higher-order accurate numerical schemes that minimizes the numerical viscosity and preserves the variation in larger-scale eddies from cycle to cycle [23][24][25].

In this study, a DISI engine CFD model was developed within a RANS framework to ensure quick turn-around time, aiming at practical engineering application. Multi-cycle simulations were performed to capture the CCV and the results were validated against experimental data at several operating conditions. The transition from non-knocking to knocking condition was observed through a spark timing sweep study. The key objective is to develop an efficient approach to predict KLSA, which can be further used to investigate fuel properties impact on knock mitigation and thermal efficiency improvement. While several approaches to predict engine knock have been proposed in literature, our approach can be easily extended to different engine platforms and fuel blends of interest.

ENGINE SPECIFICATIONS AND OPERATING CONDITIONS

The engine modeled in this study is a 1.6 L Ford EcoBoost engine operated with the production turbocharging and center-mounted direct injection fueling systems at Oak Ridge National Laboratory (ORNL). The fuel injection starts during the intake stroke, and forms a quasi-homogeneous, stoichiometric fuel/air mixture before the spark ignition. The fuel used in the experiment was an alkylate gasoline with RON of 98 and MON of 96.6. External EGR was not used. The engine geometry details can be found in Table 1.

Table 1. Engine specifications

Engine	Ford 1.6 L EcoBoost
Bore / stroke	79.0 mm / 81.3 mm
Connecting rod length	133 mm
Compression ratio	10.1 : 1
Fueling system	Center-mounted, direct injection, production injector
Injection pressure	130 bar
Start of injection	-300° aTDC
Fuel	Alkylate gasoline (RON/MON: 98/96.6)

The details of engine operating conditions are presented in Table 2, which include a slightly boosted condition with 11.5 bar indicated mean effective pressure (IMEP), and a throttled condition with 7.5 bar IMEP. The spark timing was set at the KLSA, which was determined in the experiments as the timing right before a significant increase was observed in the knock meter reading when gradually advancing the spark discharge. A spark timing sweep across the experimental KLSA point was also performed for the 11.5 bar IMEP condition for model validation purpose.

Table 2. Engine operating conditions

Engine speed (rpm)	2000	2000
IMEP (bar)	11.5	7.5
Intake manifold pressure (bar)	1.12	0.79
Exhaust manifold pressure (bar)	1.29	1.14
Spark timing (° aTDC)	-10.18, -13.47, -14.23 (KLSA), -15.21	-23 (KLSA)
Fuel mass (mg/cycle)	27.4	18.2

MODELING APPROACH

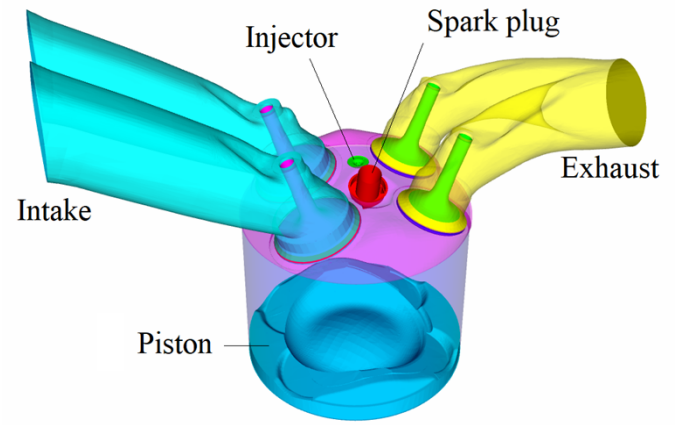

Figure 1. Engine geometry used for simulations

The engine CFD simulations were performed using a commercial software, Converge v2.3 [16]. The engine geometry was measured by x-ray scan and used in the simulations, as shown in Figure 1. A modified cut-cell Cartesian grid generation method was applied to automatically generate the computational grid at runtime. The base mesh size was set to be 2 mm. A 1 mm mesh refinement was applied for the in-cylinder region and a 0.125 mm mesh refinement was applied for the near spark region. Adaptive mesh refinement of 0.5 mm was enabled for the locations where the sub-grid velocity is above 1 m/s or sub-grid temperature is above 2.5 K. The total cell count varies during a full engine cycle and peaks at 1.3 million near bottom dead center (BDC), due to the change of in-cylinder volume and velocity and temperature field. A re-normalized group (RNG) k-ε model [26] was used to model the turbulent flow. Temperature wall function by O'Rouke and Amsden [27] was used to model the wall heat transfer. The temperatures for each wall component are summarized in Table 3, which were estimated based on a conjugated heat transfer (CHT) study on a DISI engine [28]. The fuel injection process was modeled using a Lagrangian spray model [29], in that the liquid fuel is injected as Lagrangian parcels with initial size of effective orifice radius. The Kelvin-Helmholtz Rayleigh-Taylor (KH-RT) model [30] and No Time Counter (NTC) model [31] were used to account for drop breakup and collision, respectively. The drop vaporization was modeled by Frossling correlation [27]. The alkylate fuel used in the experiments is a low octane sensitivity (1.4) fuel, and therefore was modeled as a PRF surrogate consisting of 97.3% iso-octane and 2.7% n-heptane by volume to match the anti-knock index (AKI).

Table 3. In-cylinder wall temperatures obtained from CHT calculations

Cylinder head	500 K
Liner	450 K
Piston	450 K
Intake valve	550 K
Exhaust valve	600 K

The level set G-equation model was used for modeling turbulent premixed combustion. According to the flamelet modeling theory by Peters [32], under both the corrugated flamelet and thin reaction zone regimes, the inner reactive-diffusive layer of the flame thickness can be modeled as an interface of infinitesimal thickness, which is tracked by solving the transport equation of a passive, non-reacting scalar G [33],

$$\frac{\partial \rho \tilde{G}}{\partial t} + \frac{\partial \rho \tilde{u_i} \tilde{G}}{\partial x_i} = -D_t \kappa \left| \frac{\partial \tilde{G}}{\partial x_i} \right| + \rho_u s_t \left| \frac{\partial \tilde{G}}{\partial x_i} \right| \quad (1)$$

where ~ denotes the favre-averaged mean value. ρ and ρ_u are the densities of burnt and unburnt flamelet sides, respectively. D_t is the turbulent diffusivity and κ is the mean flame front curvature. s_t is the turbulent flame speed, and can be calculated using a turbulent burning velocity relationship for RANS turbulence models [34],

$$s_t = s_l + u' \left\{ -\frac{a_4 b_3^2}{2b_1} Da + \left[\left(\frac{a_4 b_3^2}{2b_1} Da \right)^2 + a_4 b_3^2 Da \right]^{1/2} \right\} \quad (2)$$

where u' is the turbulent velocity fluctuation, s_l is the laminar flame speed, and Da is the Damkohler number. a_4, b_1 and b_3 are modeling constants [16]. Thus, the mean flame front is defined as the iso-surface where $G(x,t) = 0$ from the solution of Equation 1, while $G < 0$ indicates unburnt region and $G > 0$ indicates burnt region. The ignition process was modeled by directly sourcing G value in a spherical volume with radius of 0.5 mm located between the spark gap.

A tabular laminar flame speed model [15] was applied to evaluate s_l. In this approach, the Converge 1D solver is used to

calculate the laminar flame speed *a priori*, and generate a look-up table of s_l as function of temperature (T), pressure (P), equivalence ratio (ϕ) and dilution fraction (γ). Then this look-up table is used in the engine CFD simulation to calculate laminar flame speed based on local flow condition using appropriate interpolation scheme. Details about the laminar flame speed tabulation and interpolation scheme are presented in Table 4. The table interval and interpolation schemes ensure less than 1.5% error in laminar flame speed calculation within the tabulation range compared to the 1D calculation. Power law correlations were used to provide reasonable estimation when condition is outside of the table range, which is rarely the case for the operating conditions in this study. The exponents were determined by curve fitting against 1D calculations. A reduced PRF mechanism consisting of 109 species and 543 reactions [35] was employed for the 1D calculations. This approach is promising to provide improved accuracy than the empirical correlation approaches [36][37], and more importantly, is easy to extend for any fuel blend of interest, provided a reduced chemical kinetic mechanism exists for the blend.

Table 4. Details about laminar flame speed tabulation and interpolation

	Rang	Interval	Interpolation	Correlation
Temperature [K]	500-1500	100	Linear	$T < 500,\ s_l(T,P,\phi,\gamma) = s_l(500,P,\phi,\gamma) * (T/500)^{1.8}$
				$T > 1500,\ s_l(T,P,\phi,\gamma) = s_l(1500,P,\phi,\gamma) * (T/1500)^{3.7}$
Pressure [bar]	10-70	5	Linear	$P < 10,\ s_l(T,P,\phi,\gamma) = s_l(T,10,\phi,\gamma) * (P/10)^{-0.22}$
				$P > 70,\ s_l(T,P,\phi,\gamma) = s_l(T,70,\phi,\gamma) * (P/70)^{-0.22}$
Equivalence ratio [-]	0.5-2	0.1	Quadratic	$\phi < 0.5,\ s_l(T,P,\phi,\gamma) = s_l(T,P,0.5,\gamma) * (\phi/0.5)^{3}$
				$\phi > 2,\ s_l(T,P,\phi,\gamma) = s_l(T,P,2,\gamma) * (\phi/2)^{-3}$
Dilution fraction [-]	0-0.2	0.1	Linear	-

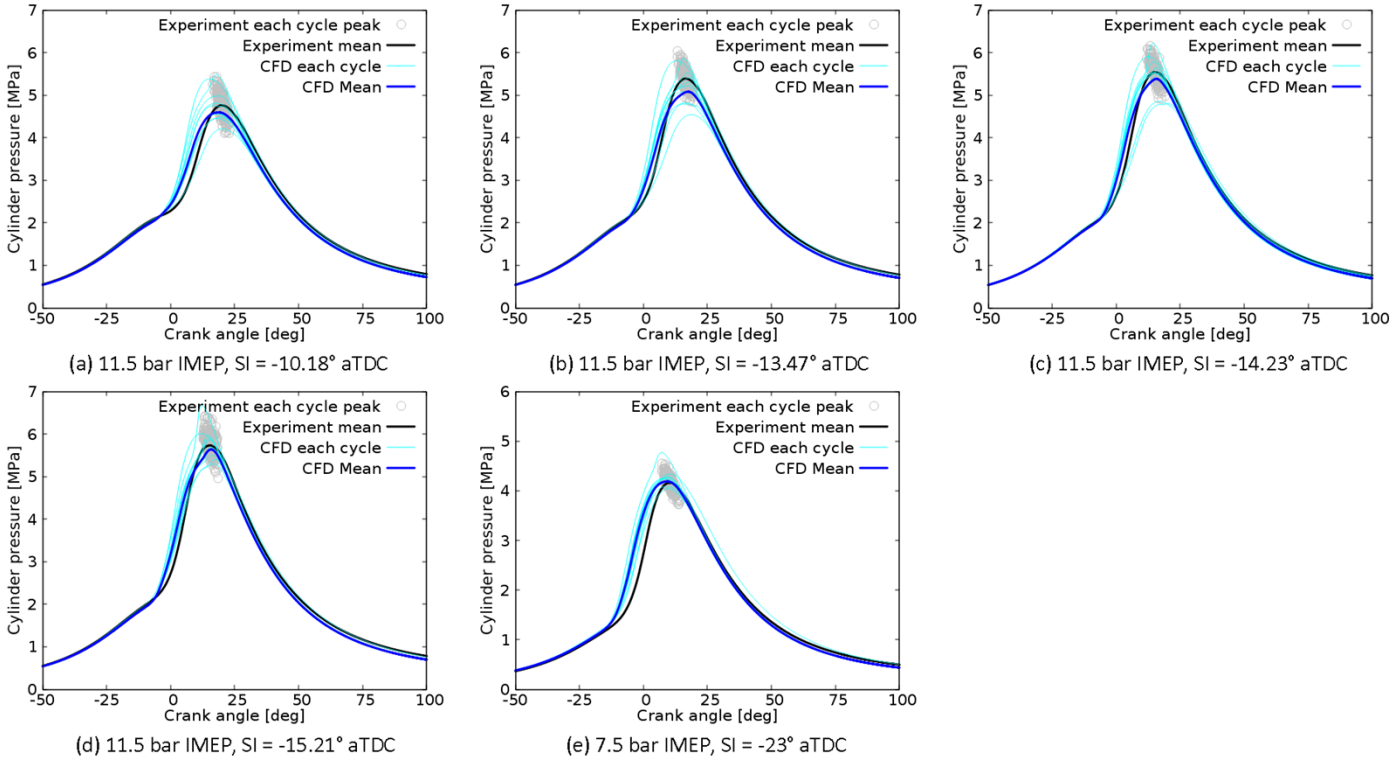

Figure 2. Measured and predicted pressure traces. Black lines are mean values of 300 cycle experimental measurements. Grey circles are the peak pressure point for each cycle. Dark blue lines are mean values of 3rd to 10th cycles CFD predictions. Light blue lines are each cycle CFD predictions.

Engine knock is a phenomenon of end gas auto-ignition before propagating flame arrival. Therefore, in order to predict knock in engine CFD simulation, the well-stirred reactor (WSR) model with detailed chemistry was applied to the unburnt region in couple with the G-equation model. To be consistent with the calculation of laminar flame speeds, the PRF

mechanism [35] was also applied to well-stirred reactor chemical kinetics calculation. This mechanism has been validated extensively for engine combustion applications and provides accurate predictions for laminar flame speed, ignition delay, species profile, etc. A Multi-zone approach [38] was used to accelerate the chemical kinetic calculations by grouping computational cells with bins of 5 K in temperature and 0.05 in equivalence ratio. Usually a Mach CFL number of 1 is suggested in engine simulation to accurately predict the pressure field and capture the knock onset. However, in this study the maximum Mach CFL number was set to be 50 to allow larger CFD time step and faster run time. An approach to still capture knock with higher CFL numbers will be demonstrated later in this paper. We believe that this is a unique contribution to the existing literature on knock predictions using CFD.

MODEL VALIDATIONS

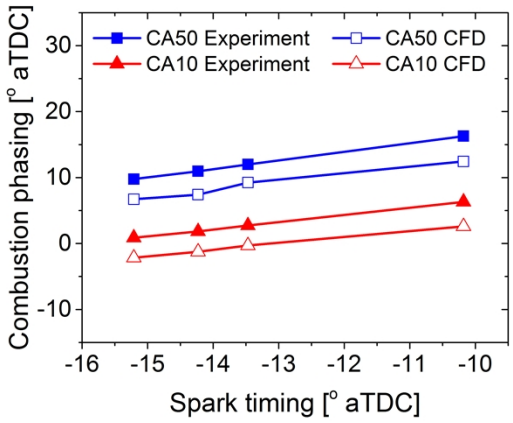

Figure 3. CA10 and CA50 as function of spark timing for 11.5 bar IMEP condition. Closed symbol lines are experimental data; open symbol lines are CFD predictions.

10 consecutive open-cycle simulations were performed for each condition, and the predicted pressure traces in comparison with experimental measurements are plotted in Figure 2. The thin lines colored in light blue are the CFD predictions for each cycle and the thick lines in dark blue are the mean values of 3rd to 10th cycles. The first two cycles are discarded from analysis to avoid influence from simulation initialization. The experimental data were measured for 300 cycles at each condition and the mean values are plotted as the black lines. The grey circles indicate the locations and magnitudes of each cycle peak pressure. A good agreement can be found between the prediction and the measurement showing that the averaged results match each other very well for all load conditions and spark timings. The predicted pressure rise is slightly earlier than the measurement, which can also be observed by comparing the CA10 and CA50, as presented in Figure 3. The CFD simulation consistently predicts a slightly early combustion phasing, which can be attributed to the use of the simple ignition model. The process from energy deposition to kernel formation and spark channel stretching are simplified by directly sourcing G value in a spherical volume, which could lead to early kernel development. The prediction of ignition process can be potentially improved by using a more detailed ignition model [39][40], however at an expense of increased computational time. Nonetheless, the simple model is computationally efficient, and is shown to provide reasonably good accuracy in predicting the location and value of peak pressure. Additionally, the trend in combustion phasing with spark timing sweep is also well captured, which is important in KLSA prediction. With advanced spark timing, the combustion phasing is advanced towards TDC, and it leads to more efficient thermal energy-to-work conversion with reduced energy loss through wall heat transfer and exhaust. However, advancing spark timing also promotes knock propensity, which will be discussed in the next section.

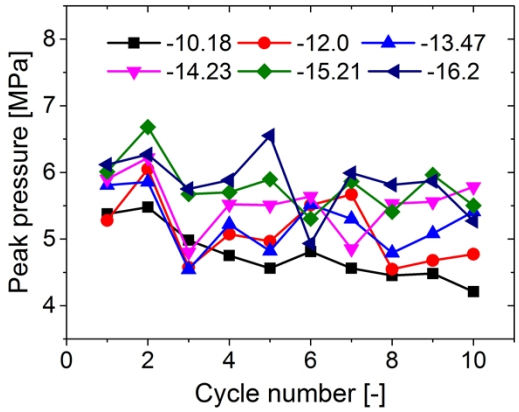

Figure 4 Peak pressures at 11.5 bar IMEP condition. Each line represents a spark timing as indicated by the legend.

The predicted peak pressure at each cycle for the spark timing sweep at 11.5 bar IMEP is presented in Figure 4 and is seen to fluctuate stochastically from cycle to cycle without converging to a stable value, suggesting that CCV is captured in the current 10-cycle RANS simulations. It is found that the second cycle is always a high cycle with the highest peak pressure among 10-cycle results, which is believed to be caused by the simulation initialization. To remove the influence from initialization, the first and second cycles are discarded from discussion.

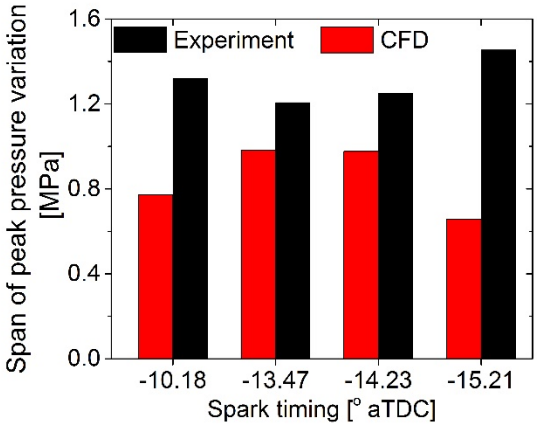

Figure 5. Span of peak pressure variation for 11.5 bar

IMEP condition. Black columns are experimental data; red columns are CFD predictions.

Figure 5 compares the measured and predicted span of peak pressure variation. It is seen that the predicted CCV is about 50% to 80% of the measured value. The source of CCV in these simulations is considered to be variations in the turbulent flow field that affects the initial kernel development

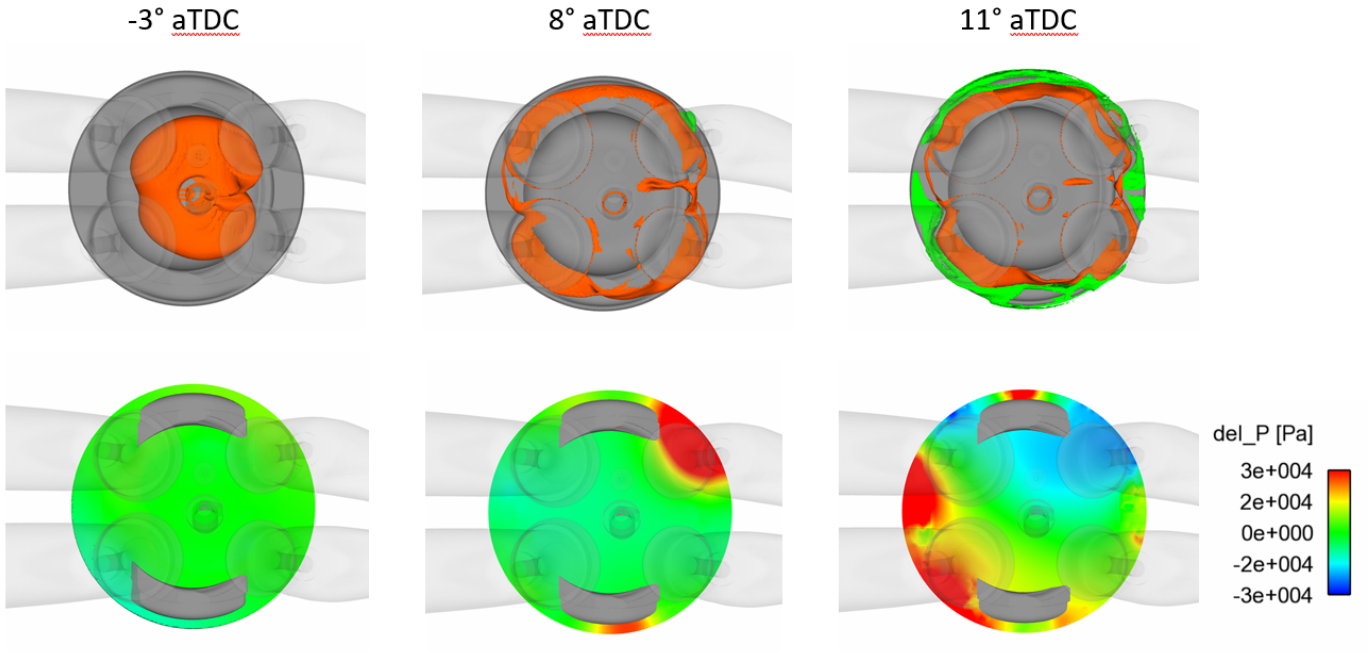

Figure 6. Visualization of in-cylinder process for a knocking case (8th cycle, 11.5 bar IMEP and -16.2° aTDC spark timing). Top row: the orange surface is the iso-surface of G=0; the green surface is the iso-surface of 2000 K in the unburnt end-gas. Bottom row: clip plane close to the cylinder head, colored by the difference between local pressure and global mean pressure.

and flame propagation, and variations in the residual gas that affect the calculation of laminar flame speed, as well as fuel/air mixing process. As discussed in the literatures reviewed previously [23][24][25], larger-scale eddies may not be damped out by the RANS. In fact, due to the turbulent viscosity with refined mesh resolution with AMR, and 2nd-order spatial discretization scheme, cycle-to-cycle variations are not being damped out, which has traditionally been the case with coarse mesh calculations in the past. We believe that LES would be a better tool to fully capture CCV, however, it is very expensive as well. Sufficiently resolved RANS simulation is able to predict CCV and help capture the extreme condition for knock prediction, although the predicted range of variation in pressure is lower than experimental measurements.

PREDICTION OF KNOCK AND KLSA

A knocking condition can be achieved by advancing the spark timing beyond the KLSA point, which is -14.23° after top dead center (aTDC) for the 11.5 bar IMEP condition in the experiment. An example of in-cylinder process at three crank angles is given in Figure 6 for a knocking case of 8th cycle of operating condition with 11.5 bar IMEP and -16.2° aTDC spark timing, which has a moderate KI among the knocking cycles. In the top row, the surface colored in orange is the iso-surface of G equals 0, representing the propagating flame front, and the surface in green is the iso-surface of temperature equals 2000 K in the unburnt end-gas ($G < 0$). In the bottom row, a clip plane is created right below the cylinder head, and the color contour indicates ΔP, which is the pressure difference between the local value and the global mean value. The intake valves are on the left side and the exhaust valves are on the right side in the figures. At -3° aTDC, the spark-ignited flame grows without any hot-spot in the unburnt region, elevating the in-cylinder pressure uniformly. The flame is slightly offset from the center towards the exhaust side, reflecting the tumble flow direction. At 8° aTDC, as the flame keeps growing and compressing the end-gas, a hot-spot is observed at the location close to the cylinder head and exhaust valve, indicating the knock onset. Correspondingly, a sharp pressure rise is also established at the same location. Following the knock onset, the end-gas is rapidly consumed by the auto- ignition event, accompanied by pressure waves oscillating inside of the cylinder, as can be seen at 11° aTDC.

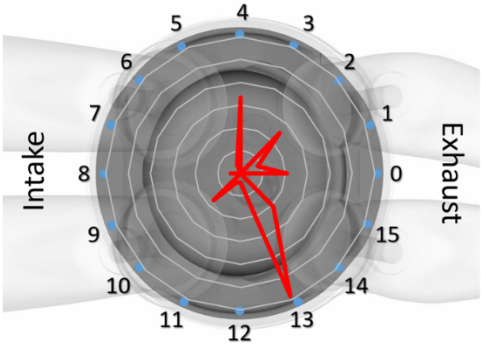

Figure 7 Monitor point location and radar chart of PDF for maximum pressure oscillation location.

To quantify the KI, 16 monitor points were set along the liner right below the cylinder head to record local pressure, as indicated by the blue dots in Figure 7. MAPO analysis was then performed with a band filter of 4-20 kHz to obtain the pressure oscillation that is relevant to knock [15]. An example of pressure oscillation is given as black line in Figure 8 (a), which is the maximum pressure oscillation in the same engine cycle as shown in Figure 6 with 11.5 bar IMEP and -16.2° aTDC spark timing. The end-gas heat release rate is also plotted as black line in Figure 8 (b) to illustrate the end-gas auto-ignition process. A low temperature heat release is firstly observed following the spark discharge from -10 to 0° aTDC, and negligible pressure oscillation is seen within this duration. A sharp increase in the end-gas heat release due to high temperature reaction is then found at ~10° aTDC suggesting the occurrence of end-gas auto-ignition. At the same time, the rapid heat release results in significant fluctuation in the pressure field, as can be seen in Figure 8 (a). The KI is defined as the maximum absolute value of peak pressure oscillations among all the monitor point locations. A probability density function (PDF) of the maximum pressure oscillation location from 48 simulation runs for the 11.5 bar IMEP condition is shown in Figure 7. It is seen that the maximum pressure oscillation is most likely to be found at locations that close to the exhaust valve. The high temperature of exhaust valve has a strong impact on the end-gas heat release and knock onset that a hot spot tends to form on the exhaust side, which is also observed in Figure 6.

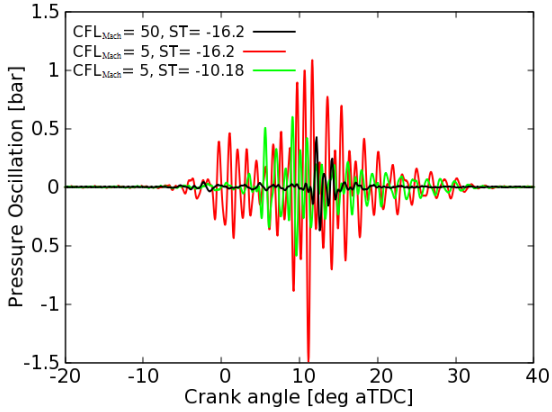

(a) Maximum pressure oscillation

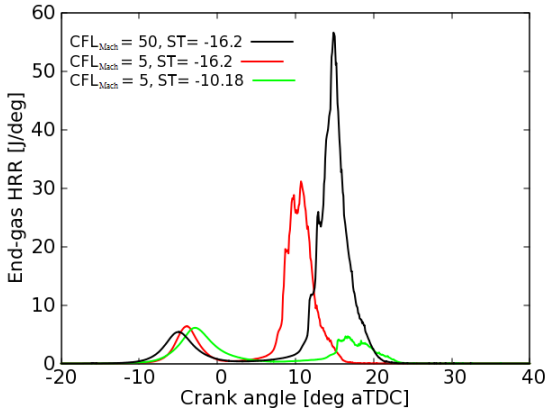

(b) End-gas heat release rate

Figure 8. Simulation results for three cases at 11.5 bar IMEP condition with varying Mach CFLs and spark timings.

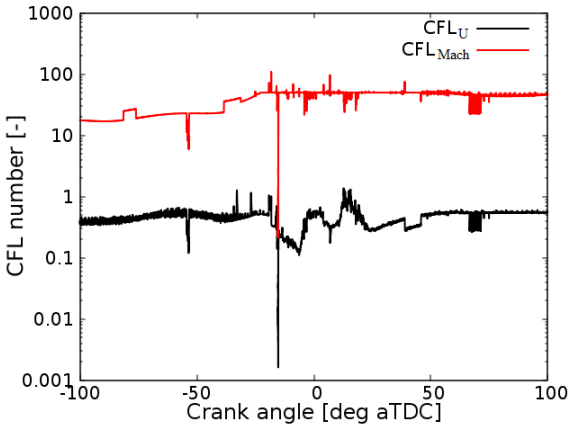

Figure 9. Calculated convective CFL (CFL_U) and Mach CFL (CFL_{Mach}) from CFD simulation.

As mentioned previously, the simulations in this study use a maximum Mach CFL number of 50, which does not mean that a fixed Mach CFL is used, but the CFD time step is limited from yielding a Mach CFL larger than 50 while the time step is also subjected to other restrictions [16]. An example of calculated maximum Mach CFL for the 8th cycle of 11.5 bar IMEP, -16.2° aTDC spark timing condition is provided in Figure 9 in comparison with calculated convective CFL. The Mach CFL is defined as $CFL_{mach} = c\Delta t/\Delta x$. c is the local speed of sound, Δt is the time step, and Δx is the local length scale. Convective CFL is defined similarly as Mach CFL, but is calculated with the flow velocity (U) instead of speed of sound (c). It is seen that the convective CFL is consistently lower than 1, which ensures a stable solution for the Navier-Stokes equation. The Mach CFL is lower than the specified value of 50 during the compression stroke, where the time step is limited by other factors, such as spray, diffusion calculations, or excessive iterations in the Pressure-Implicit with Splitting of Operators (PISO) procedure, etc. The significant downward spikes in both

convective CFL and Mach CFL around -16.2° aTDC indicate very small time steps (1~5*10^{-8} s) caused by the start of sourcing G value during the spark discharge. Following that, the Mach CFL becomes the limiting factor and stabilizes around 50.

A Mach CFL less than 1 is usually suggested to accurately capture a pressure wave. Two more simulation results are presented in Figure 8 (a) and (b) to illustrate the sensitivity of pressure oscillation prediction on Mach CFL number. The red lines are results with spark timing at -16.2° aTDC, and the green lines are results with spark timing at -10.18° aTDC. Both cases use a Mach CFL number of 5. As can be seen in Figure 8 (b), the early spark discharge at -16.2° aTDC using small CFL also leads to a knocking cycle, as indicated by the high temperature heat release, while the late spark timing at -10.18° aTDC is a much more stable condition. However, both cases with small Mach CFL present higher intensity of pressure oscillation compared to the case with large Mach CFL, despite the fact that the green lines represent a non-knocking condition. Thus, determining knock onset by a threshold value in the pressure oscillation is somewhat arbitrary, and strongly depends on the Mach CFL. While use of a small Mach CFL number less than 1 is expected to achieve convergence in pressure oscillation prediction, it is also extremely computational expensive, especially when multi-cycle simulation is desired for SI engine study. Applying Mach CFL of 1 or 5 only for the combustion duration (-20 ~ 50° aTDC) while keeping Mach CFL as 50 for the rest of the cycle, requires longer simulation time by a factor of 3 or 1.4, respectively, compared to using Mach CFL of 50 throughout the simulation for the current CFD model setup.

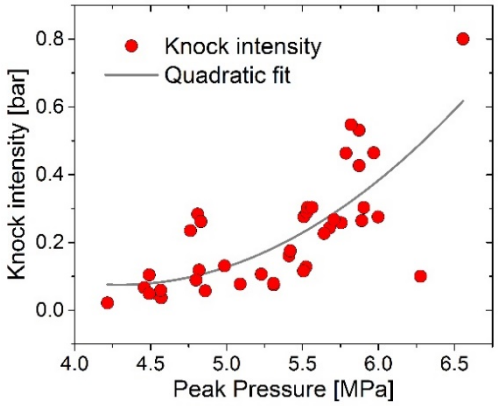

Figure 10. KI vs. Peak pressure for 11.5 bar IMEP condition. Red dots represent each cycle result. The grey line is a quadratic regression fitting curve.

Moreover, the prediction of knock propensity is complicated by CCV of SI combustion. Figure 10 plots the KI against peak pressure for each cycle simulation at 11.5 bar IMEP condition. A strong correlation exists between the KI and the peak pressure that higher peak pressure often leads to stronger KI, as indicated by the grey line, which is a quadratic curve from regression fitting. In other words, there is also some level of cyclic variation in the predicted KI, as in the peak pressure. Thus, single-cycle simulation is not enough to reflect its knock propensity even when the averaged experimental result is well matched. Multi-cycle simulation is then required to capture the extreme case in the KI prediction.

Figure 11 plots the KI at each cycle as function of spark timing for both load conditions. As seen in Figure 11 (a), the extrema points are highlighted as red line, which can be divided into two sections: a flat section from -10.18 to -13.47° aTDC, representing non-knocking conditions, and a steep section from -13.47° aTDC and beyond, representing knocking conditions with increased KI as spark timing advanced. Therefore, instead of using an absolute threshold value, the non-dimensional trend of KI extrema is examined, and the slope change point in the KI extrema is shown be to a good indicator of the knock onset point, i.e., KLSA. This approach predicts a KLSA of -13.47° aTDC, which is very close to the experimental KLSA of -14.23° aTDC. Similar trend is also found for the 7.5 bar IMEP condition, and the slope change point predicts a KLSA of -23° aTDC, which is the same to the experimental measurement. The accuracy of KLSA prediction can be affected by the spark timing sweep interval. The currently used 1 crank angle degree (CAD) interval is considered to be sufficient since the change in IMEP with spark timing around KLSA is less than 0.7% per CAD for the studied cases.

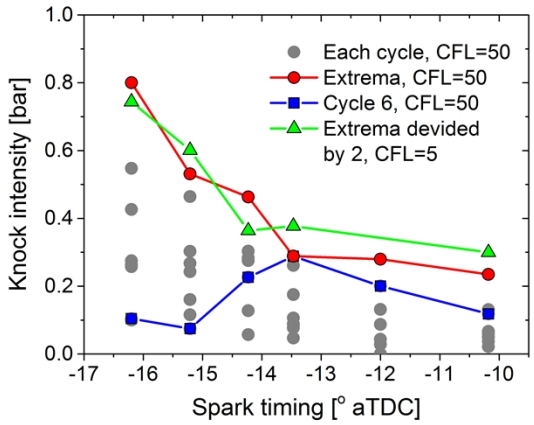

(a) 11.5 bar IMEP

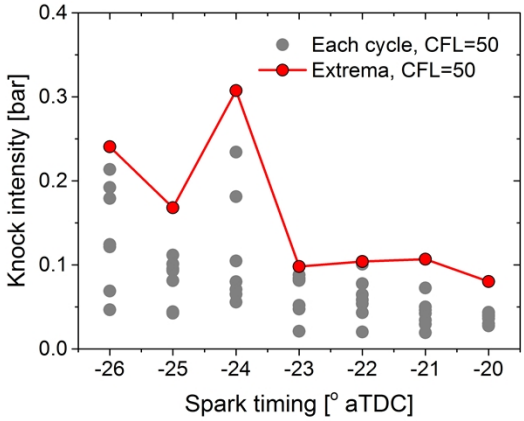

(b) 7.5 bar IMEP

Figure 11. KI as function of spark timing. Grey dots represent KI at each cycle. Red line is the KI extrema and

blue line is the KI of 6th cycle using Mach CFL of 50. Green line is the prediction using Mach CFL of 5, divided by a factor of 2.

The blue line in Figure 11 (a) is the KI prediction at cycle 6, which shows a completely different trend, suggesting that single-cycle simulation can not be used alone to identify the KLSA and multi-cycle results are needed to account for the influence of CCV on the KI prediction. The current 10-cycle simulation is a best practice for the two load conditions in this study to attain a reliable and stable trend in the KI extrema. Additionally, the simulation results with Mach CFL of 5 is also plotted as green symbol line in Figure 11 (a). Although the absolute value of KI predicted using CFL of 5 and CFL of 50 are different by a factor of 2, the trends are quite similar, both suggesting a KLSA at around -14.23 ~ -13.47° aTDC by the slope change points. Therefore, the proposed approach is shown to be less sensitive to the Mach CFL, and also accounts for influence of CCV.

SUMMARY AND CONCLUSIONS

A CFD simulation study of cyclic variability and knock prediction in a boosted SI engine was performed. G-equation combustion model coupled with well-stirred reactor model was used to capture the turbulent flame propagation and end-gas auto-ignition. A simple ignition model was used and shown to give reasonably good prediction. A RANS turbulence model with a large Mach CFL number of 50 were used to keep the computation efficient and relevant to engineering application. 10 consecutive engine cycle simulation was performed and validated against experimental data with several operating loads and spark timings. Good agreement between simulation and experiment can be found in terms of averaged pressure traces and combustion phasing. It is shown that the current multi-cycle RANS simulation is able to represent the CCV from experimental measurement. The CCV observed in this study is considered due to the use of a fine mesh and high-order spatial discretization scheme which preserves the large-scale flow structures and their variations from cycle to cycle.

Engine knock was induced in the simulation by advancing the spark timing beyond the KLSA point. The end-gas is consumed by the auto-ignition rapidly after the knock onset, accompanied by significant pressure wave fluctuating inside of the cylinder, as illustrated by the 3D in-cylinder visualization. MAPO analysis with a 4 to 20 kHz band filter was employed to quantify the KI, which shows a significant dependency on the Mach CFL number, imposing difficulties in determining knock onset by using an absolute threshold value in KI. Also, a strong correlation was found between the peak pressures and the maximum knock intensities, suggesting a similar level of variation in the KI as in the peak pressure. To address these difficulties, a new approach to predict KLSA is proposed, which uses the slope change point in the KI extrema from multi-cycle simulation as an indicator of KLSA. This approach accurately predict the KLSA for the studied condition, and is also shown to be insensitive to the Mach CFL number, and also accounts for cyclic variability effects with a relatively low computational cost.

ACKNOWLEDGEMENTS

UChicago Argonne, LLC, operator of Argonne National Laboratory ("Argonne"), a U.S. Department of Energy Office of Science laboratory, is operated under Contract No. DE-AC02- 06CH11357. The U.S. Government retains for itself, and others acting on its behalf, a paid-up nonexclusive, irrevocable worldwide license in said article to reproduce, prepare derivative works, distribute copies to the public, and perform publicly and display publicly, by or on behalf of the Government. This research was partially funded by DOEs Office of Vehicle Technologies, Office of Energy Efficiency and Renewable Energy under Contract No. DE-AC02-06CH11357. The authors wish to thank Gurpreet Singh, Michael Weismiller, and Kevin Stork, program managers at DOE, for their support. This research was conducted as part of the Co-Optimization of Fuels & Engines (Co-Optima) project sponsored by the U.S. Department of Energy (DOE) Office of Energy Efficiency and Renewable Energy (EERE), Bioenergy Technologies and Vehicle Technologies Offices.

The authors would like to acknowledge the HPC center at the National Renewable Energy Laboratory (NREL) for computing resource on the Peregrine cluster and the Laboratory Computing Resource Center (LCRC) at Argonne National Laboratory (ANL) for computing resource on the Blues cluster that were used in this research.

REFERENCE

[1] https://www.eia.gov/totalenergy/data/monthly/

[2] ASTM International, 2012, "Standard Test Method for Research Octane Number of Spark-Ignition Engine Fuel," ASTM International, West Conshohocken, PA. Standard No. ASTM D2699-12.

[3] ASTM International, 2016, "Standard Test Method for Motor Octane Number of Spark-Ignition Engine Fuel," ASTM International, West Conshohocken, PA. Standard No. D2700-16.

[4] Kalghatgi, G. T., 2001, "Fuel Anti-knock Quality- Part I, Engine Studies," SAE Paper No. 2001-01-3584.

[5] Kalghatgi, G. T., 2001, "Fuel Anti-knock Quality- Part I, Vehicle Studies- How Relevant is Motor Octane Number (MON) for Modern Engines?," SAE Paper No. 2001-01-3585.

[6] Yates, A. D., Swarts, A., and Viljoen, C., 2005, "Correlating Auto- Ignition Delays and Knock-Limited Spark Advance Data for Different Types of Fuel," SAE Paper No. 2005-01-2083.

[7] Amer, A., Babiker, H., Chang, J., Kalghatgi, G. T., et al., 2012, "Fuel effects on knock in a highly boosted direct injection spark ignition engine," SAE Int. J. Fuels Lubr. 5(3) pp. 1048–1065.

[8] Sluder, C. S., Szybist, J. P., McCormick, R. L., Ratcliff, M. A., Zigler, B. T., 2016, "Exploring The Relationship Between Octane Sensitivity and Heat-of-Vaporization," SAE Int. J. Fuels Lubr., 9(1), pp. 80-90.

[9] Szybist, J. P., and Splitter, D. A., 2016, "Pressure and temperature effects on fuels with varying octane

sensitivity at high load in SI engines," Combust. Flame, 177, pp. 49–66.

[10] Eckert, P., Kong, S., and Reitz, R., 2003, "Modeling Autoignition and Engine Knock Under Spark Ignition Conditions," SAE Paper No. 2003-01-0011.

[11] Liang, L., Reitz, R., Iyer, C., and Yi, J., 2007, "Modeling Knock in Spark-Ignition Engines Using a G-equation Combustion Model Incorporating Detailed Chemical Kinetics," SAE Paper No. 2007-01-0165.

[12] Shao, J., and Rutland, C., 2014, "Modeling Investigation of Auto- ignition and Engine Knock by HO2," SAE Paper No. 2014-01- 1221.

[13] Shao, J., and Rutland, C. J., 2014, "Modeling Investigation of Different Methods to Suppress Engine Knock on a Small Spark Ignition Engine," J. Eng. Gas Turb. Power, 137(6), pp. 61506.

[14] Pan, J., Wei, H., Shu, G., Pan, M., Feng, D., and Li, N., 2017, "LES analysis for auto-ignition induced abnormal combustion based on a downsized SI engine," Appl. Energy, 191, pp. 183-192.

[15] Pal, P., Wu, Y., Lu, T., Som, S., See, Y. C., Le Moine, A., 2018, "Multidimensional Numerical Simulations of Knocking Combustion in a Cooperative Fuel Research Engine," ASME J. Energy Resour. Technol., 140, p. 102205.

[16] CONVERGE 2.3 Theory Manual, Convergent Science Inc., Middleton, WI, 2016.

[17] Heywood, J. B., 1988, "Internal Combustion Engine Fundamentals," McGraw-Hill, New York.

[18] Vermorel, O., Richard, S., Colin, O., Angelberger, C., Benkenida, A., and Veynante, D., 2007, "Multi-Cycle LES Simulations of Flow and Combustion in a PFI SI 4-Valve Production Engine," SAE Paper No. 2007- 01-0151.

[19] Granet, V., Vermorel, O., Lacour, C., Enaux, B., Dugue´, V., and Poinsot, T., 2012, "Large-Eddy Simulation and experimental study of cycle-to-cycle variations of stable and unstable operating points in a spark ignition engine," Combust. Flame 159(4), pp. 1562-1575.

[20] Schmitt, M., Hu, R., Wright, Y. M., Soltic, P., and Boulouchos, K., 2015, "Multiple Cycle LES Simulations of a Direct Injection Natural Gas Engine," Flow Turbul. Combust., 95(4), pp. 645–668.

[21] Zhao, L., Moiz, A. A., Som, S., Fogla, N., Bybee, M., Wahiduzzaman, S., Mirzaeian, M., Millo, F., and Kodavasal, J., 2017, "Examining the Role of Flame Topologies and In-Cylinder Flow Fields on Cyclic Variability in Spark-Ignited Engines Using Large-Eddy Simulation," Int. J. Eng. Res., https://doi.org/10.1177/1468087417732447

[22] Ameen, M. M., Mizaeian, M., Millo, F., and Som, S., 2018, "Numerical Prediction of Cyclic Variability in a Spark Ignition Engine Using a Parallel Large Eddy Simulation Approach," ASME J Energy Resour. Technol. 140(5) p. 052203.

[23] Richards, K., Probst, D., Pomraning, E., Senecal, P. K., and Scarcelli, R., 2014, "The Observation of Cyclic Variation in Engine Simulations When Using RANS Turbulence Modeling," ASME. Internal Combustion Engine Division Fall Technical Conference, doi:10.1115/ICEF2014-5605.

[24] Scarcelli, R., Richards, K., Pomraning, E., Senecal, P. et al., 2016, "Cycle-to-Cycle Variations in Multi-Cycle Engine RANS Simulations," SAE Paper No. 2016-01-0593.

[25] Battistoni, M., Grimaldi, C., Cruccolini, V., Discepoli, G. et al., 2017, "Assessment of Port Water Injection Strategies to Control Knock in a GDI Engine through Multi-Cycle CFD Simulations," SAE Paper No. 2017-24-0034.

[26] Han, Z., and Reitz, R. D., 1995, "Turbulence Modeling of Internal Combustion Engines Using RNG κ-ε Models," Combust. Sci. Technol., 106(4–6), pp. 267–295.

[27] Amsden, A.A., 1997, "KIVA-3V: A Block Structured KIVA Program for Engines with Vertical or Canted Valves," Los Alamos National Laboratory Technical Report LA-13313-MS.

[28] Leguille, M., Ravet, F., Le Moine, J., Pomraning, E., Richards, K., and Senecal, P. K., 2017, "Coupled Fluid-Solid Simulation for the Prediction of Gas- Exposed Surface Temperature Distribution in a SI Engine," SAE Paper No. 2017-01-0669.

[29] Reitz, R. D., 1987, "Modeling atomization processes in high-pressure vaporizing sprays," Atomization Spray Technology, 3, pp. 309–337.

[30] Beale, J. C. and Reitz, R. D., 1999, "Modeling spray atomization with the Kelvin-Helmholtz/Rayleigh-Taylor hybrid model," Atomization Spray, 9(6), pp. 623–650.

[31] Schmidt, D. P. and Rutland, C. J., 2000, "A New Droplet Collision Algorithm," J. Comput. Phys., 164(1), pp. 62-80.

[32] Peters, N, 1986, "Laminar Flamelet Concepts in Turbulent Combustion," Symposium (International) on Combustion, 21(1), pp. 1231-1250.

[33] Tan, Z. and Reitz, R. D., 2003, "Modeling Ignition and Combustion in Spark-ignition Engines Using a Level Set Method," SAE Paper No. 2003-01-0722.

[34] Peters, N., 2000, Turbulent Combustion, Cambridge University Press, Cambridge, UK.

[35] Wang, H., Yao, M., Yue, Z., Jia, M., and Reitz, R. D., 2015, "A reduced toluene reference fuel chemical kinetic mechanism for combustion and polycyclic-aromatic hydrocarbon predictions," Combust. Flame, 162(6), pp. 2390–2404.

[36] Metghalchi, M. and Keck, J.C., 1982, "Burning Velocities of Mixtures of Air and Methanol, Isooctane and Indolene at High Pressures and Temperatures," Combust. Flame, 48, pp. 191-210.

[37] Gulder, O.L., 1984, “Correlations of Laminar Combustion Data for Alternative S.I. Engine Fuels,” SAE Paper No. 841000.

[38] Babajimopoulos, A., Assanis, D.N., Flowers, D.L., Aceves, S.M., and Hessel, R.P., 2005, “A Fully Coupled Computational Fluid Dynamics and Multi-zone Model With Detailed Chemical Kinetics for the Simulation of Premixed Charge Compression Ignition Engines,” Int. J. Engine Res., 6, pp. 497–512.

[39] Dahms, R.N., Drake, M.C., Fansler, T.D., Kuo, T.-W., Peters, N., 2011, “Understanding ignition processes in spray-guided gasoline engines using high-speed imaging and the extended spark-ignition model SparkCIMM. Part A: Spark channel processes and the turbulent flame front propagation,” Combust. Flame, 158, pp. 2229–2244.

[40] Colin, O., Truffin, K., 2011, “A spark ignition model for large eddy simulation based on an FSD transport equation (ISSIM-LES),” Proc. Combust. Inst., 33(2), pp. 3097-3104.